Two-Dimensional Coarsening Kinetics of Reconstruction Domains: GaAs(001)-$\beta(2 \times 4)$

V. M. Kaganer, W. Braun, B. Jenichen, L. Däweritz, and K. H. Ploog

Paul-Drude-Institut für Festkörperelektronik, Hausvogteiplatz 5–7, D-10117 Berlin, Germany
(Received 1 August 2002; published 6 January 2003)

We study the nonconserved coarsening kinetics of a reconstructed semiconductor surface. The domain size evolution is obtained *in situ* by time-resolved surface x-ray diffraction. The system exhibits four equivalent domain types with two nonequivalent types of domain boundaries. Small domains are prepared by molecular beam epitaxy deposition of one GaAs layer. We find the correlation lengths of the domain size distribution to depend on time as $l \propto t^{0.42 \pm 0.05}$ in the half-order reflections and $l \propto t^{0.22 \pm 0.05}$ in the quarter-order reflections. The fraction of the higher energy domain boundaries increases as ln$t$.

A system quenched into a nonequilibrium polydomain state tries to reduce the total energy of the domain interfaces by increasing the sizes of individual domains. Lifshitz [1] and Allen and Cahn [2] showed that, if the domain coarsening is not restricted by a conservation law, the average domain size l increases in time as $l(t) \propto t^n$, with an exponent $n = 1/2$ in both two- and three-dimensional systems. Lifshitz [1] pointed out that the coarsening law can be qualitatively different if the number of the equivalent domain types m is larger than 2 ($m \geq 3$ in 2D and $m \geq 4$ in 3D), since the junction points of several domain boundaries may pin the domain boundary. Numerous computer simulations on the standard (Ising, Potts, *XY*, planar rotor) models have shown the universality of the exponent $1/2$ in two-state and multi-state systems (for a review, see Refs. [3,4]). Although most of the numerical simulations were performed on two-dimensional models, the domain coarsening kinetics in two-dimensional systems with nonconserved order parameter was the subject of only very few experimental works. We are aware of studies on just one system, a chemisorbed oxygen monolayer on a tungsten surface, by low energy electron diffraction [5–7].

In the present paper, we report time-resolved x-ray diffraction studies of the coarsening kinetics of the $\beta(2 \times 4)$ reconstruction domains on the GaAs(001) surface. If a weak ordering along the short axis of the unit cell is neglected, the system possesses $m = 4$ equivalent translational domains (90° rotational domains are absent since the surface is polar) with two nonequivalent types of boundaries between the domains [8].

The measurements were performed at the PHARAO beam line at the synchrotron BESSY II (Berlin, Germany) in a combined molecular beam epitaxy (MBE)/6-circle diffractometer system dedicated to the *in situ* x-ray scattering analysis of III-V semiconductors. Standard MBE sample preparation procedures were used. From the rocking curve of the integer-order surface reflection 1 3 0.05, we obtain a mean terrace width $l = 2/\Delta q$ [where Δq is the full width at half maximum (FWHM) deconvolved with the instrumental resolution]

of approximately 450 nm, which agrees with atomic force microscopy measurements of one of the samples.

X-ray diffraction allows for a separate study of the reconstruction domains in fractional-order reflections and the surface morphology in integer-order reflections [9], since the reconstruction domains differ by translations being multiples of the bulk lattice spacing and are not seen in the integer-order reflections. Figure 1 compares real time x-ray diffraction measurements during MBE growth at these two types of reflections. The integer-order measurements (top curve) reveal intensity oscillations during deposition [10,11]. In the fractional-order reflection (bottom curve), the diffracted intensity is almost zero during deposition, and the recovery after the deposition is much slower compared to the integer-order reflection. Very similar behavior of the fractional-order peak was reported in an x-ray diffraction study of organometallic vapor-phase epitaxy of GaAs [12] and treated as the absence of surface reconstruction during growth. In our experiment, the $\beta(2 \times 4)$ reconstruction is continuously seen in simultaneous reflection high-energy electron diffraction, although weaker during deposition.

For a quantitative study of reconstruction domain coarsening, we deposit one layer of GaAs. During the deposition, two-dimensional islands nucleate, grow in size by incorporating further adatoms, and coalesce. We
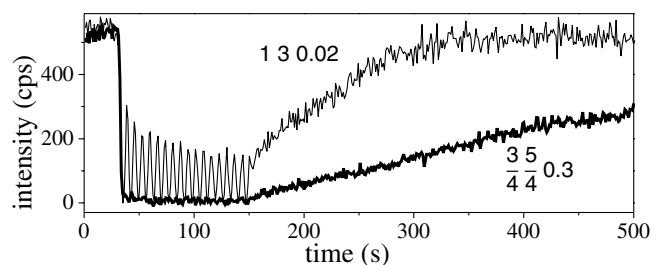
FIG. 1. Time-resolved x-ray intensities at an integer order reflection (top) and at a fractional-order reflection (bottom). Here, as in all subsequent figures, the measured intensity is normalized to a storage ring current of 100 mA and the background is subtracted.

can expect that the reconstruction develops independently on each island. The deposition of one layer results in a flat surface with as many reconstruction domains as two-dimensional islands were nucleated during the deposition. The inset of Fig. 2(c) shows the kinetics of the surface morphology. The drop and subsequent increase of the intensity during deposition of a single layer corresponds to the first oscillation seen in the integer-order reflection in Fig. 1. Within 30 s after the layer is deposited, the intensity is recovered, and the surface is flat again. This is an instantaneous process compared to the intensity recovery in the fractional-order reflections [Fig. 2(c)]. We have chosen the half- and quarter-order reflections along the 4× axis of the 2 × 4 unit cell and reflections close to the 2× axis [Fig. 2(b)] since the ordering along the short axis is weak and the fractional-order reflections $[h\bar{h}]$ have low intensities [8].

Intensity variations during the recovery in Fig. 2(c) are the result of interference between different reconstruction

domains. The intensity increases due to domain coarsening and finally reaches a maximum when the domain sizes exceed the resolution of the x-ray diffraction experiment. Then, the different domains add incoherently to the total signal. This interpretation is verified in Figs. 2(d) and 2(e), which present ω scans during recovery and the integrated intensities of the reflections, respectively. The ω scans were obtained by stepwise rotation of the sample about its normal. One scan takes approximately 75 s. The ω steps were chosen nonuniformly, with a smaller spacing near the peak position, which allowed one to measure both wide peaks at the beginning of recovery and narrow peaks at its end. The ω scans were fitted to Voigt functions with the width of the Gaussian component fixed by the resolution and a variable width of the Lorentzian component. The resolution was obtained separately for each reflection by interpolating between the peak widths of the 200, 220, and 400 in-plane bulk reflections. The ω scan of the 220 reflection is shown in
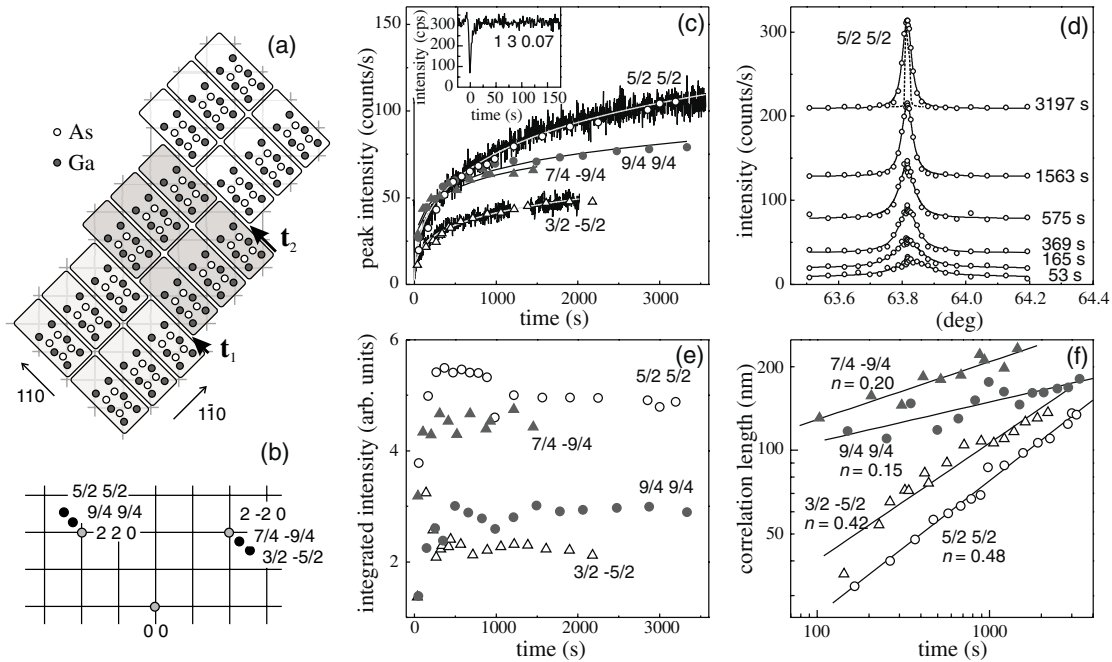
FIG. 2.   (a) Unit cells and domains of the $\beta(2 \times 4)$ reconstruction. Only the top As and Ga layers are shown. The characteristic feature of this reconstruction is the rows of missing As dimers, commonly seen as grooves on scanning tunneling microscope (STM) images. The boundaries between reconstruction domains are two nonequivalent stacking faults, $\mathbf{t}_1 = \pm\frac{1}{2}[110]$ and $\mathbf{t}_2 = [110]$, seen as kinks of the grooves in STM. The square mesh represents the termination of the bulk GaAs(001) surface. (b) Fractional order reflections chosen for the present study (black dots) and the nearest bulk reflections (gray dots). (c) Time dependence of the peak intensities after the deposition of one layer of GaAs. Uneven lines represent the measured peak intensities of the half-order reflections. Symbols are the peak intensities obtained from ω scans during the recovery. Smooth lines are fits to Eq. (1). The inset shows the kinetics of two-dimensional islands measured in an integer-order reflection. (d) ω scans performed during the recovery. The time at each curve shows the moment of the measurement of the center of the curve. The broken line at the top curve is an ω scan of the bulk reflection 220 used as the resolution. The solid lines are the Voigt function fits to the experimental data. The curves are shifted vertically for clarity. (e) Time dependence of the integrated intensities obtained from the Voigt fits shown in the ω scans. The integrated intensity of the $\frac{7}{4}\frac{9}{4}$ reflection is increased by a factor of 2. (f) Time dependence of the correlation lengths $l = 2/\Delta q$ obtained from the FWHMs Δq of the Lorentzian components of the Voigt function. The exponents n of the power law $l \propto t^n$ are shown for each reflection. The measurements were performed in the reciprocal space points $\frac{5}{2}\frac{5}{2}0.1$, $\frac{9}{2}\frac{9}{2}0.1$, $\frac{3}{2}\frac{5}{2}0.2$, and $\frac{7}{4}\frac{9}{4}0.2$. The in-plane Miller indices of the reflections are given in the figure, the third index is omitted for simplicity. The substrate temperature is 530 °C, the V/III flux ratio during deposition is 2, the growth rate is 0.2 ML/s.

Fig. 2(d) by a broken line. The peak of the first ω scan after the deposition [bottom curve in Fig. 2(d)] is shifted to larger scattering angles, which corresponds to a compressive strain along the surface of 8×10^{-4} in the reconstructed domains on the initial stage of recovery. This strain may be caused by domain boundaries playing an essential role for small domains, and by steps bounding two-dimensional islands still present at this stage of recovery.

The integrated intensity of each reflection changes only during the initial 300 s, Fig. 2(e), which can be explained by contributions from the domain boundaries covering a noticeable part of the surface when the domains are small. At later times, the integrated intensity does not change in time, as expected: This is the quantity used in structure analysis since it does not depend on the domain size. We conclude that, during recovery, the atomic structure of the reconstructed unit cell and the area of the reconstructed surface do not change.

Figure 2(f) presents the correlation lengths $l(t) = 2/\Delta q(t)$ obtained from the FWHMs $\Delta q(t)$ of the Lorentzian components of the Voigt fits shown in Fig. 2(b). The correlation lengths follow a power law, $l(t) \propto t^n$, with notably different exponents of half- and quarter-order reflections, given in Fig. 2(f). The exponents can be independently obtained by fitting the time dependence of the peak intensity $I(t)$ [Fig. 2(c)]. The convolution of a Lorentzian peak profile with a Gaussian resolution function at the peak maximum is

$$I(t) = I_0 \exp[(l_c/2l)^2] \, \text{erfc}(l_c/2l). \tag{1}$$

Here $\text{erfc}(x)$ is the complementary error function, $I_0 = \mathcal{I} l_c/(4\sqrt{\pi})$ is the peak intensity maximum corresponding to scattering from infinitely large domains, $\mathcal{I}$ is the integrated intensity of the reflection, and l_c is the x-ray coherence length. The smooth curves in Fig. 2(c) are fits of the measured peak intensities to Eq. (1) with $l(t) = l_c(t/\tau)^n$. The exponent n and the time constant τ are the only fit parameters, since the integrated intensity $\mathcal{I}$ and the coherence length l_c are known from independent measurements. From these fits, we obtain somewhat smaller exponents than in Fig. 2(f) for the half-order reflections (0.40 and 0.35 for $\frac{5}{2}\frac{5}{2}$ and $\frac{3}{2}\frac{5}{2}$ reflections, respectively), and somewhat larger exponents for quarter-order reflections (0.25 and 0.30 for $\frac{9}{4}\frac{9}{4}$ and $\frac{7}{4}\frac{9}{4}$ reflections, respectively). On average, we obtain coarsening exponents of 0.42 ± 0.05 for the half-order reflections and 0.22 ± 0.05 for the quarter-order reflections.

Figure 2(f) also reveals an anisotropy in the reconstruction domain shapes: The correlation lengths obtained in the [110] direction are approximately 1.5 times smaller than in the perpendicular direction. Hence, the reconstruction domains extend along the long axis of the 2×4 unit cell. This is in contrast to the morphology of the two-dimensional islands, which are usually elongated in the perpendicular direction.

The ratio $R = l_{1/4}/l_{1/2}$ of the correlation lengths obtained in the quarter- and half-order reflections in the same direction decreases from 3 at the initial stage of recovery to almost 1 at the end [Fig. 2(f)]. The systematically larger peak widths (and correspondingly smaller correlation lengths) of the half-order reflections are the result of the different extinction conditions for half- and quarter-order reflections [8]. The elementary stacking fault between reconstruction domains $\mathbf{t}_1 = \pm\frac{1}{2}[110]$ [single kink in the As dimer rows, Fig. 2(a)] gives rise to a phase factor $\exp(i\pi/2)$ in quarter-order reflections and $\exp(i\pi)$ in half-order reflections. The domains differing by the elementary translation interfere entirely destructively in half-order reflections and only partially destructively in quarter-order reflections. Hence, the x-ray intensity recovers faster in the quarter-order reflections. The simplest model of the domain distribution [8], with the probability of a domain boundary depending only on the state of the preceding unit cell, leads to exponential correlation functions with the correlation lengths differing by no more than a factor of $R = 2$ between quarter- and half-order reflections, with the largest factor reached when only the elementary stacking faults $\mathbf{t}_1$ are present. However, our experiments give a larger factor of $R \approx 3$ at the initial stage of the recovery [Fig. 2(f)].

Our aim now is to show that the correlation length ratio R can be larger than in the case of the most disordered domain distribution considered in Ref. [8]. We extend the analysis by decoupling the probabilities of different domain boundaries from the domain size distribution. We introduce a probability p of the stacking faults $\mathbf{t}_1 = \pm\frac{1}{2}[110]$ and the probability $1 - 2p$ of a stacking fault $\mathbf{t}_2 = [110]$. The domain size distribution $P(x)$ is taken the same for all four types of domains, since the domains are equivalent. Its Fourier transform $C(q)$ is the characteristic function of the size distribution.

The problem of x-ray scattering from a sequence of reconstruction domains is mathematically equivalent to the problem of scattering from a terraced surface, with the phase differences between domains corresponding to surface steps. An effective method to calculate the scattered intensity is to consider the terrace (domain), rather than the surface atom (unit cell), as an elementary scattering object [13]. The problem can then be solved analytically in closed form if the probability of a domain boundary depends only on the state of the preceding domain. Applying the method of Ref. [13], we obtain the diffraction peak profiles for half- and quarter-order reflections as

$$I_{1/2} = \text{Re} \frac{4p(1 - C)}{[1 + (4p - 1)C]q^2},$$

$$I_{1/4} = \text{Re} \frac{2(1 - p)(1 - C)}{[1 + (1 - 2p)C]q^2}. \tag{2}$$

The model of Ref. [8] is described by $C(q) = 1/(1 + iql)$.
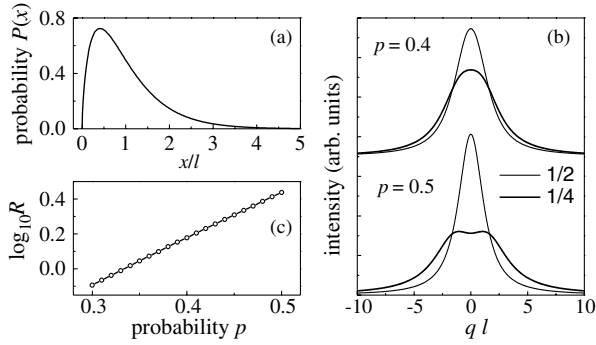
FIG. 3. (a) The probability distribution $P(x)$ of the gamma distribution with the parameter $M = 1.6$. (b) Half- and quarter-order peak profiles calculated from Eq. (2) with this probability distribution $p = 0.5$ (the domain boundaries t_1 only) and $p = 0.4$. (c) The ratio $R = l_{1/4}/l_{1/2}$ of the correlation lengths obtained from the calculated peak profiles versus p.

Substituting this expression into Eq. (2), we obtain Lorentzian peaks with a width ratio of $\Delta q_{1/2}/\Delta q_{1/4} = 2p/(1 - p)$, which reaches a maximum of 2 when p reaches its maximum $p = 0.5$ [8].

A better model for the domain size distribution is the gamma distribution [14]. Its only parameter M allows one to proceed smoothly from the exponential distribution [8] at $M \to 1$ to domains of equal width l at $M \to \infty$. Figure 3(a) shows the gamma distribution at $M = 1.6$. Its characteristic function $C(q) = [1 + (ql/M)^2]^{-M/2} \times \exp[iM \arctan(ql/M)]$ is used to calculate the peak profiles by Eq. (2) [see Fig. 3(b)]. The maximum of the ratio R is reached with $p = 0.5$, i.e., when only the domain boundaries t_1 are present. This result can be understood qualitatively by considering the opposite limit, when only the boundaries t_2 are present. Then, all domains would scatter in phase in a half-order reflection, resulting in its quick recovery. In a quarter-order reflection, the domains would contribute destructively (phase difference π), giving rise to a slow recovery, in contrast to our observations. The peak width ratio R is equal to 2.9 at $p = 0.5$, which is close to the experimentally observed ratio at the initial stage of the recovery.

Therefore, at the initial stage of the recovery, the t_2 boundaries are absent and the domain size distribution is rather broad, albeit with low probability of very small domains [cf. Fig. 3(a)]. The reason for the appearance of the t_2 boundaries is obvious. If a sequence of domains $1-2-3$ separated by t_1 boundaries is present at the initial stage of coarsening, the growth of the domains 1 and 3 at the expense of the domain 2 gives rise to a t_2 domain boundary $1-3$. An increasing probability of t_2 domain boundaries gives rise to smaller peak width ratios [Fig. 3(b) and 3(c)]. The dependence of R on p, obtained from Lorentzian fits of the calculated peak profiles, is close to exponential [Fig. 3(c)]. Taking into account that the correlation lengths depend on time through power laws [Fig. 2(f)] we conclude that the fraction of t_2 domain boundaries increases as the logarithm of time. This is of course a rough estimate, since R varies only by a factor of 3 within the experimentally accessible time interval. It shows, however, that the probability of the translation to half of the reconstructed unit cell, $t_2 = [110]$, increases slowly compared to the domain size kinetics.

In conclusion, we find that two-dimensional multidomain systems with energetically nonequivalent domain boundaries show a slower coarsening compared to the standard Lifshitz-Allen-Cahn theory. The system under investigation, $\beta(2 \times 4)$-reconstructed GaAs(001) surface, possesses four equivalent translational domains with two nonequivalent types of boundaries between the domains. Using *in situ* x-ray diffraction, we find that the growth of the reconstruction domains is described by two different time exponents: the correlation length increases as $l \propto t^{0.42 \pm 0.05}$ in the half-order reflections and $l \propto t^{0.22 \pm 0.05}$ in the quarter-order reflections. Introducing an improved model for the domain size distribution, we conclude that the fraction of the higher energy domain boundaries increases as the logarithm of time. The surface reconstruction domains are anisotropic with an aspect ratio of 1.5 and extended along [110], orthogonal to the long axis of the morphological surface anisotropy.

[1] I. M. Lifshitz, Zh. Eksp. Teor. Fiz. **42**, 1354 (1962) [Sov. Phys. JETP **15**, 939 (1962)].
[2] S. M. Allen and J. W. Cahn, Acta Metall. **27**, 1085 (1979).
[3] O. G. Mouritsen, *Kinetics of Ordering and Growth at Surfaces* (Plenum, New York, 1990), p. 1.
[4] A. J. Bray, Adv. Phys. **43**, 357 (1994).
[5] G.-C. Wang and T.-M. Lu, Phys. Rev. Lett. **50**, 2014 (1983).
[6] P. K. Wu, J. H. Perepezko, J. T. McKinney, and M. G. Lagally, Phys. Rev. Lett. **51**, 1577 (1983).
[7] M. C. Tringides, P. K. Wu, and M. G. Lagally, Phys. Rev. Lett. **59**, 315 (1987).
[8] Y. Garreau, M. Sauvage-Simkin, N. Jedrecy, R. Pinchaux, and M. B. Veron, Phys. Rev. B **54**, 17638 (1996).
[9] E. Vlieg, J. F. van der Veen, S. J. Gurman, C. Norris, and J. E. Macdonald, Surf. Sci. **210**, 301 (1989).
[10] E. Vlieg, A. W. Denier van der Gon, J. F. van der Veen, J. E. Macdonald, and C. Norris, Phys. Rev. Lett. **61**, 2241 (1988).
[11] P. H. Fuoss, D. W. Kisker, F. J. Lamelas, G. B. Stephenson, P. Imperatori, and S. Brennan, Phys. Rev. Lett. **69**, 2791 (1992).
[12] F. J. Lamelas, P. H. Fuoss, P. Imperatori, D. W. Kisker, G. B. Stephenson, and S. Brennan, Appl. Phys. Lett. **60**, 2610 (1992).
[13] B. Croset and C. de Beauvais, Surf. Sci. **409**, 403 (1998).
[14] P. R. Pukite, C. S. Lent, and P. I. Cohen, Surf. Sci. **161**, 39 (1985).